



Mapping Inter-individual Functional Connectivity Variability in TMS Targets for Major Depressive Disorder

Shreyas Harita^{1,2}, Davide Momi², Frank Mazza^{2,3} and John D. Griffiths^{1,2,4*}

¹ Institute of Medical Science, University of Toronto, Toronto, ON, Canada, ² Krembil Centre for Neuroinformatics, Centre for Addiction and Mental Health (CAMH), Toronto, ON, Canada, ³ Department of Physiology, University of Toronto, Toronto, ON, Canada, ⁴ Department of Psychiatry, University of Toronto, Toronto, ON, Canada

OPEN ACCESS

Edited by:

Martin J. Hermann,
Julius Maximilian University of
Würzburg, Germany

Reviewed by:

Michel J. A. M. van Putten,
University of Twente, Netherlands
Daniel Keeser,
Ludwig Maximilian University of
Munich, Germany

*Correspondence:

John D. Griffiths
john.griffiths@utoronto.ca

Specialty section:

This article was submitted to
Neuroimaging and Stimulation,
a section of the journal
Frontiers in Psychiatry

Received: 22 March 2022

Accepted: 23 May 2022

Published: 23 June 2022

Citation:

Harita S, Momi D, Mazza F and
Griffiths JD (2022) Mapping
Inter-individual Functional Connectivity
Variability in TMS Targets for Major
Depressive Disorder.
Front. Psychiatry 13:902089.
doi: 10.3389/fpsy.2022.902089

Transcranial magnetic stimulation (TMS) is an emerging alternative to existing treatments for major depressive disorder (MDD). The effects of TMS on both brain physiology and therapeutic outcomes are known to be highly variable from subject to subject, however. Proposed reasons for this variability include individual differences in neurophysiology, in cortical geometry, and in brain connectivity. Standard approaches to TMS target site definition tend to focus on coordinates or landmarks within the individual brain regions implicated in MDD, such as the dorsolateral prefrontal cortex (dlPFC) and orbitofrontal cortex (OFC). Additionally considering the network connectivity of these sites (i.e., the wider set of brain regions that may be mono- or poly-synaptically activated by TMS stimulation) has the potential to improve subject-specificity of TMS targeting and, in turn, improve treatment outcomes. In this study, we looked at the functional connectivity (FC) of dlPFC and OFC TMS targets, based on induced electrical field (E-field) maps, estimated using the SimNIBS library. We hypothesized that individual differences in spontaneous functional brain dynamics would contribute more to downstream network engagement than individual differences in cortical geometry (i.e., E-field variability). We generated individualized E-field maps on the cortical surface for 121 subjects (67 female) from the Human Connectome Project database using tetrahedral head models generated from T1- and T2-weighted MR images. F3 and Fp1 electrode positions were used to target the left dlPFC and left OFC, respectively. We analyzed inter-subject variability in the shape and location of these TMS target E-field patterns, their FC, and the major functional networks to which they belong. Our results revealed the key differences in TMS target FC between the dlPFC and OFC, and also how this connectivity varies across subjects. Three major functional networks were targeted across the dlPFC and OFC: the ventral attention, fronto-parietal and default-mode networks in the dlPFC, and the fronto-parietal and default mode networks in the OFC. Inter-subject variability in cortical geometry and in FC was high. Our analyses showed that the use of normative neuroimaging reference data (group-average or representative FC and subject E-field) allows prediction of which networks are targeted, but fails to accurately quantify the relative loading of TMS targeting on each of the principal networks. Our results characterize the FC patterns of canonical therapeutic TMS targets, and the key dimensions of their variability across subjects. The

high inter-individual variability in cortical geometry and FC, leading to high variability in distributions of targeted brain networks, may account for the high levels of variability in physiological and therapeutic TMS outcomes. These insights should, we hope, prove useful as part of the broader effort by the psychiatry, neurology, and neuroimaging communities to help improve and refine TMS therapy, through a better understanding of the technology and its neurophysiological effects.

Keywords: TMS, functional connectivity, E-fields, modeling, human, depression

HIGHLIGHTS

- E-field modeling and functional connectivity used to study TMS targets (dlPFC, OFC).
- Considerable variability in TMS target E-field patterns seen across subjects.
- Large inter-subject differences in target connectivity observed and characterized.
- Major functional networks targeted by dlPFC, OFC TMS were the VAN, FPN and DMN.
- Insights can contribute to improved and more personalized TMS therapies in the future.

INTRODUCTION

TMS Stimulation Therapy Targets and the Neurobiology of Major Depressive Disorder

A considerable number of patients with major depressive disorder (MDD) do not respond to first-line therapies such as drugs or psychotherapy (1). People who fail to respond to two or more pharmacological interventions of a sufficient dose and time are characterized as having treatment-resistant depression [TRD; (2)]. Transcranial magnetic stimulation (TMS) is an efficacious and cost-effective treatment for people with TRD and is an emerging alternative to existing treatments for MDD, as well as a variety of other neurological and psychiatric disorders. However, the clinical utility of TMS remains limited by the large heterogeneity in its clinical outcomes (3). One factor believed to contribute to this variable clinical response among patients is individual differences in structural and functional brain connectivity (4). In order to find a target site for TMS treatment, seed-based approaches have focused on individual brain regions implicated in MDD, such as the dorsolateral prefrontal cortex (dlPFC), dorsomedial prefrontal cortex (dmPFC), and orbitofrontal cortex (OFC). On the other hand, network-based approaches have shown how TMS efficacy can be improved by considering not only the location of the primary stimulation site (dlPFC, OFC, etc.), but also its connectivity - i.e., the wider set of distal brain regions that are mono- or poly-synaptically activated by TMS stimulation (5, 6).

Previous studies have shown that variability in clinical efficacy of dlPFC-targeted repetitive TMS (rTMS) treatment for MDD is related to differences in the functional connectivity (FC) of the specific dlPFC locations stimulated [see (7, 8)]. These observations suggest that a detailed examination of individual differences in FC patterns for frontal lobe rTMS targets should

prove useful in further refining TMS targeting methodologies. The aim of the present study was to undertake such an examination. Specifically, we characterized the FC patterns of the dlPFC and OFC, based on E-field maps generated by biophysical simulations of TMS stimulation effects on the cortex (see Section METHODS). Our hypothesis was that individual differences in spontaneous functional brain dynamics would contribute more to downstream network engagement than individual differences in cortical geometry (i.e., E-field variability), which may, in turn, explain some of the observed heterogeneity of rTMS treatment outcomes.

By far the most commonly targeted site in rTMS treatment of MDD is the dlPFC. That this region is known to play a critical role in executive functions such as attention, planning, and organization, and up-regulation of the circuits underlying these neurocognitive functions is one potential explanation for its positive therapeutic effects. rTMS stimulation of the left dlPFC has also been observed to regulate FC to and between the reward- and emotion-related regions of the mesocorticolimbic dopamine pathway, which have also been consistently implicated in MDD (9). However, stimulation of the left dlPFC does not work for all patients, with only around 46% of MDD patients achieving response, and only 31% achieving remission after a standard rTMS treatment course (10). This may be due to inter-subject differences in neurochemistry, connectivity, in their specific MDD neuropathology, or a variety of other potential factors. To overcome this issue of limited success with dlPFC targeting, several groups have begun to explore alternative rTMS targets to treat MDD, such as the dmPFC and the OFC (4).

Recent research has shown that the OFC is hyperactive in MDD (11). The OFC consists of a medial (mOFC) and a lateral (lOFC) subdivision, each with unique anatomical and FC profiles. The OFC has extensive cortico-cortical and cortico-striatal connections to regions implicated in MDD such as the cingulate cortex, caudate, striatum, hypothalamus, amygdala, hippocampus, insula, and thalamus (12). Recently, studies have begun to explore the OFC as a TMS target, with the rationale being to stimulate these MDD-implicated cortico-cortical and cortico-striatal loops. The OFC and its downstream connections are principal contributors to reward and reversal learning (13), predictive and fictive error assessment (14), emotional regulation, and generation of affective states (15). Due to the wide psychiatric implications of pathological OFC activity, this region has been growing in popularity as an alternative rTMS treatment target for mental illness. For example, low frequency (1 Hz) rTMS of the left OFC has been shown to ameliorate symptoms in patients with

obsessive-compulsive disorder (OCD; (16). Relatedly, 1Hz rTMS to the right OFC in a recent study saw nearly a quarter of patients suffering from MDD achieve remission (11). Importantly, these patients previously showed minimal response to dlPFC-rTMS. These results point to heterogeneous mechanisms of action, and therefore therapeutic effect, for dlPFC-, dmPFC-, and OFC-rTMS, possibly due to their unique downstream connections.

E-field Modeling and Cortical Geometry

Transcranial magnetic stimulation uses high-intensity magnetic field pulses to influence neuronal activity. The TMS coil produces a time-varying magnetic field, which in turn induces a focal electric field (E-field) within brain (principally cortical) tissue. E-field modeling is a relatively new approach that uses computationally estimated E-field maps, which can serve as a proxy to identify the region of the brain that is stimulated for a given coil type, location, orientation, and (MRI scan-derived, subject-specific) head and brain characteristics (17–19). These methodologies are increasingly used in clinical and basic TMS research, as a means to better understand and minimize the sources of variability in TMS outcomes due to the varying placement of TMS coils on the subject's scalp, and to variability in each individual's skull anatomy and cortical geometry.

Approaches to TMS coil placement include the “5 cm-rule,” 10–20 EEG electrode locations, MRI-guided anatomical targeting, and the more recent fMRI FC-guided targeting. However, there is a considerable amount of variability in the “ideal” TMS coil placement to optimally stimulate a specific target. For example, the F3 10–20 electrode position may result in different parts of the dlPFC being stimulated in different individuals. Moreover, previous research has shown that differences in the complex neuroanatomy of each individual human skull and brain (i.e., brain size, gyri, and sulci differences) result in E-fields of varying shapes, sizes, and depths (20). The combined effect of TMS coil placements and subject-specific differences in skull anatomy and cortical geometry leads to an inter-subject variation in E-field patterns across patients/subjects and is a potential explanation for some of the high variability in rTMS therapy outcomes. Furthermore, the interaction between this cortical geometry-driven variability in TMS-induced E-fields and variability in intrinsic FC patterns, despite receiving some attention from researchers previously (21), remains poorly understood.

Present Study

It is likely that the dlPFC and OFC have unique functional connections, through which they each exert their differential therapeutic effects following rTMS treatment (22). The patterns of these connections likely vary considerably across subjects, and very little is currently known about the relative contributions of these variability sources to TMS treatment outcomes. In this framework, even though a previous study has combined anatomically realistic finite element models of the human head with resting functional MRI to predict functional networks targeted *via* TMS at a given coil location and orientation (21), none so far have investigated the impact of the individual

subject and group-average FC patterns for a consistent E-field-defined seed region using different TMS locations. In the present study, we, therefore, sought to address part of this knowledge deficit, by systematically examining E-field and FC patterns for dlPFC and OFC TMS target sites, using structural and functional neuroimaging scans in a group of healthy control subjects. We computed simulated TMS E-fields centered at the dlPFC and OFC and studied their FC patterns using both individual and group averaged resting-state fMRI data. We found specific networks being targeted as a result of dlPFC or OFC TMS. While the same major networks were targeted consistently across our subject cohort, substantial inter-individual differences in each subject's specific relation to these networks were also observed. Comparing individual subject and group-average FC patterns for a consistent E-field-defined seed region allowed us to assess the contribution of inter-individual variability in FC patterns, independently of variability in cortical geometry. Conversely, comparing FC patterns for a single group-level E-field seed to those for subject-specific E-field seeds allowed us to quantify variability in TMS target connectivity due purely to skull and cortical geometry variation. Our results highlight the inter-individual differences in dlPFC and OFC TMS FC, potentially paving the way for personalized rTMS therapy in the future.

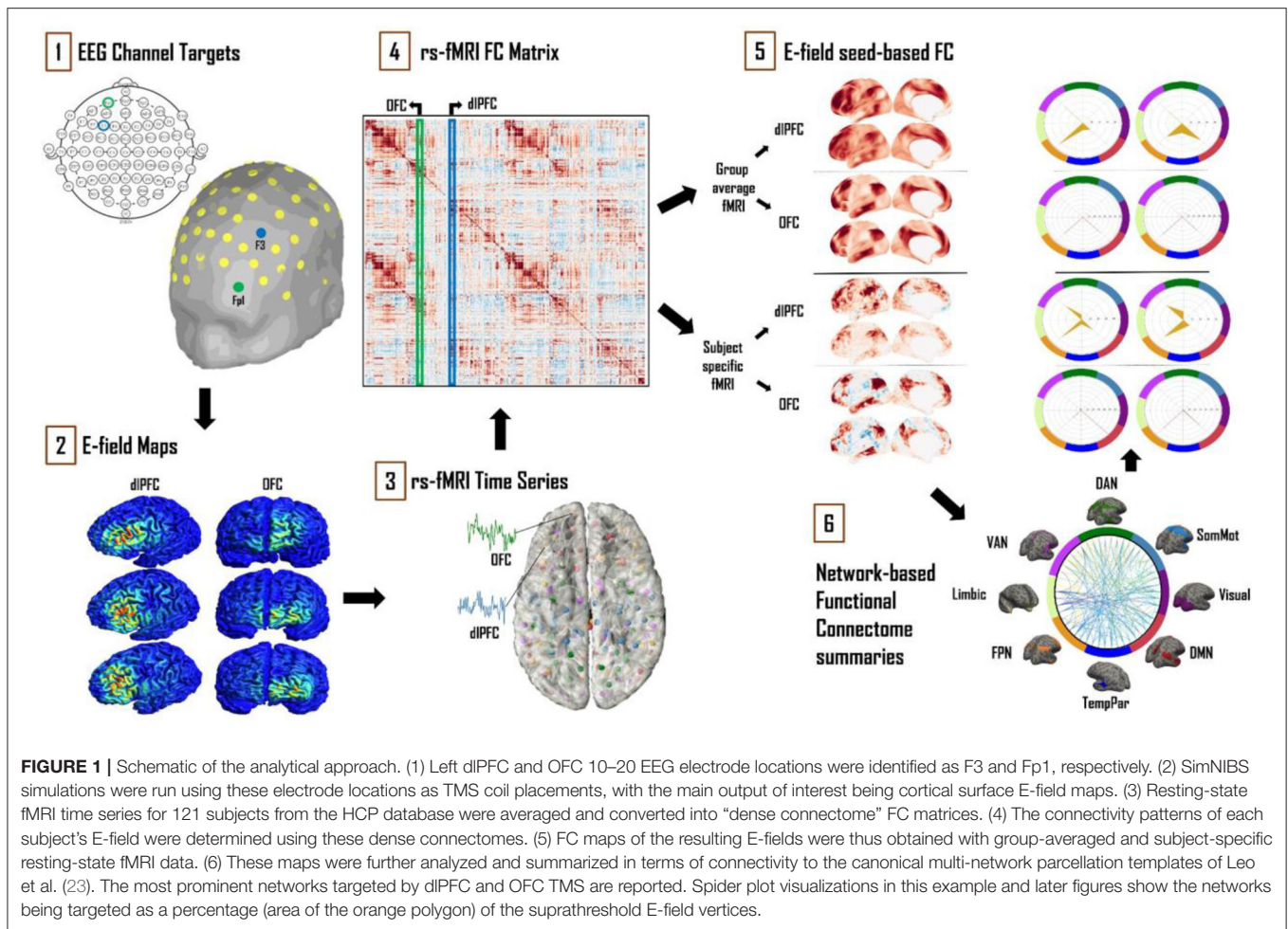
METHODS

Subjects were chosen randomly from the Human Connectome Project (HCP) database for our analysis. We selected a total of 121 subjects, of which 67 were female. All of our randomly selected subjects were young adults, with a mean age of 28.8 (min: 22 years old, max: 36 years old) years old. Out of 121 subjects, our sample contained 58 twins (32 monozygotic and 26 dizygotic).

Analysis of T1- and T2-weighted anatomical MRI (for E-fields) and fMRI (for FC) data was conducted looking specifically at FC patterns related to dlPFC and OFC TMS stimulation. We computed TMS E-fields using the SimNIBS software package and focused on the cortical surface component of the stimulated tissue. The group average and individual subject HCP CIFTI dense connectomes were used to determine the FC of TMS targets to the rest of the brain, and we used the standard Yeo/Schaefer parcellations to summarize the downstream connections of the dlPFC and OFC. Finally, we defined a framework for assessing contributions to overall variability from cortical geometry, FC, and from a combination of these two sources. Each of these steps is detailed below (**Figure 1**).

Determining the TMS E-field

The TMS-induced electric field was modeled using tools from the SimNIBS software library (17). We used the “mri2mesh” head modeling pipeline to create a tetrahedral surface mesh head model (.msh file) from T1- and T2-weighted MR images and Freesurfer tissue segmentations for all subjects. This mesh consisted of five tissue types: white matter (WM), gray matter (GM), cerebrospinal fluid (CSF), skull, and scalp. The assigned conductivity values were fixed, as per the SimNIBS defaults: 0.126 S/m (WM), 0.275 S/m (GM), 1.654 S/m (CSF), 0.01 S/m (skull), and 0.465 S/m (scalp). In order to investigate possible effects due



to head geometry, two head mesh types were used as part of the SimNIBS analysis pipeline. The first was each subject’s unique head meshes, as derived from that subject’s own neuroanatomical MRI scans. The second was the general template head mesh, “ernie.msh,” which is distributed as a part of SimNIBS. The EEG 10–20 system F3 electrode was selected to target the left dlPFC, for two reasons: First: EEG F3 is in our experience currently the most commonly used left dlPFC targeting method in clinical rTMS practices. Second: it has been reported that TMS targeting approaches based on the 10–20 EEG system account better for variability across different skull shapes and sizes than scalp-based measurements such as the “5 cm rule” (8). With regards to the OFC, previous work has shown that targeting the right OFC *via* the Fp2 electrode led to remission in MDD patients unresponsive to dlPFC- and dmPFC-rTMS (24). Given the high level of anatomical symmetry between hemispheric homologs, here we used the Fp1 electrode (left-side homolog of Fp2, thus targeting left OFC), so as to keep both TMS targets in the left hemisphere. This approach enabled us to make more direct comparisons between dlPFC and OFC, minimizing extraneous methodological differences. We strongly expect our left OFC results to generalize well to right OFC targets, although we leave the full demonstration of this for future work. The left dlPFC

has been used as a target for rTMS therapy almost since the technique’s inception (25), and while there are heterogeneous outcomes associated with left dlPFC rTMS, it is still one of the most widely used rTMS targets for MDD (8, 26). The use of the OFC as a TMS target to treat psychiatric disorders, while still a novel and largely underexplored idea, has recently gained traction - with OFC rTMS showing promise in treating MDD [right OFC; (11)] and OCD [left OFC; (16)].

At both coil centers (F3, Fp1), the coils were positioned using the standard orientation to ensure that the resulting E-field is directed perpendicularly into the cortex. Previous studies have shown that this standard orientation is able to achieve the highest perpendicular E-field values (27). This is done by pointing the coil handle away from the midline of the cortex. The y-direction position values for the dlPFC (F3) and OFC (Fp1) are therefore F5 and AF7, respectively. Of the various coil models available in SimNIBS, we used the Magstim 70 mm Figure-8 coil, which is the most common coil type in both clinical and research settings. To keep our focus primarily around the target regions (dlPFC, OFC), we used a threshold of 0.9 Volt/meter (V/m) to limit the size of the E-field obtained (28). We report the E-field sizes in units millimeter squared (mm^2), calculated directly from the faces (triangles) of the CIFTI surface meshes. For reference,

these meshes consist of 32,492 vertices and 64,980 faces per hemisphere, with an average face area of 0.05 mm².

Functional Connectivity

Resting-state fMRI data of the 121 HCP subjects was used to study the FC of TMS target regions. For full details on the HCP acquisition protocols and related information, see (29–32).

For subject-specific FC analyses, the FC for the CIFTI format time series for each HCP subject's four resting-state fMRI scans were averaged and converted into “dense connectome” (Pearson correlation) FC matrices, each containing 91,282 rows and columns (corresponding to ~64,000 cortical surface vertices, and ~27,000 sub-cortical voxels). For group-level FC analyses, the HCP_S1200_GroupAvg_v1 (1,003 subjects) dense connectome was used instead of individual-subject data. The FC of a given E-field was determined by taking the average FC, over all the vertices within that E-field, to every other node in the dense connectome FC matrix. Note that in this study we only studied connectivity within the stimulated (i.e., the left) hemisphere. In order to summarize which downstream regions were functionally connected to the stimulated areas, we grouped the connectivity profiles of dlPFC and OFC stimulation target sites according to the canonical functional network parcellation of Yeo et al. (23) and Schaefer et al. (33). These canonical networks consisted of the visual (Vis), somatomotor (SomMot), dorsal attention (DAN), ventral attention (VAN), limbic, frontoparietal (FPN), temporoparietal (TempPar), and default-mode (DMN) networks (23, 33). These canonical Yeo/Schaefer network summaries give a useful low-dimensional complement to the high-dimensional (E-field seed column-averaged) FC dense connectome columns, helping us to gain a better understanding of which functional networks might be stimulated by TMS, and how the pattern of stimulated areas varied between target sites (dlPFC, OFC) and across subjects. Here, the individual units of a Yeo/Schaefer parcellation-based functional connectome are the brain regions identified by Schaefer et al. (33), and serve as building blocks for functional brain anatomy. In the context of network analysis, each parcel represents a single node within a whole-brain network. In the following, we, therefore, refer to these individual Yeo/Schaefer parcels as network “nodes.” In all subjects, we analyzed E-field variability, FC patterns, and the major nodes of the most common functional networks and the FC maps they created.

To explore the impact of individual brain features on the variability of TMS target connectivity, we delineated a two-level FC analysis framework. At the first level (1a, 1b), the two most likely main sources of TMS FC variability are analyzed separately, and at the second level (2) they are analyzed in combination:

1a. Influence of individual head, skull, and cortical geometry on TMS target connectivity patterns. To examine this we computed the variability shown in the E-fields by holding the FC constant. To do this, we used each subject's unique head mesh to determine their individualized E-field map. As described above, the connectivity of each subject's specific E-field to the canonical HCP_S1200_GroupAvg_v1 resting-state FC matrix was studied.

1b. Inter-subject differences in TMS target connectivity due purely to each subject's unique functional connectivity profile.

This line of analysis involved using the same E-field across all subjects, but combining it with individualized FC. The SimNIBS general-template head mesh (“ernie.msh”) was used to generate a fixed E-field pattern for all subjects, for each of the two TMS targets. The connectivity patterns of this fixed E-field to the rest of the brain were calculated using each subject's individual FC matrix, derived from their four resting-state fMRI scans. This approach allowed us to measure the effect of individual spatial FC fingerprints on TMS target connectivity.

2. Combined influence of individual cortical geometry and individual functional connectivity structure on TMS target connectivity patterns. To represent the “real-world” scenario, where individual characteristics of both cortical geometry and FC jointly contribute to TMS target connectivity patterns, we combined the approaches in 1a and 1b above and studied patterns using both each subject's unique head mesh and their specific FC matrices.

Statistical Analysis

Connectivity scores were compared separately for dlPFC and OFC using repeated-measures one-way ANOVA, with the (within-subjects) factor “NETWORK” (eight levels for the eight functional networks: Vis, SomMot, DAN, VAN, Limbic, FPN, TempPar, DMN). Subsequent pairwise *post hoc* comparisons were performed to determine significant differences between NETWORK levels. The critical *p*-value was then adjusted using Tukey correction to account for multiple comparisons (**0.05; Tukey corrected; *0.05 uncorrected).

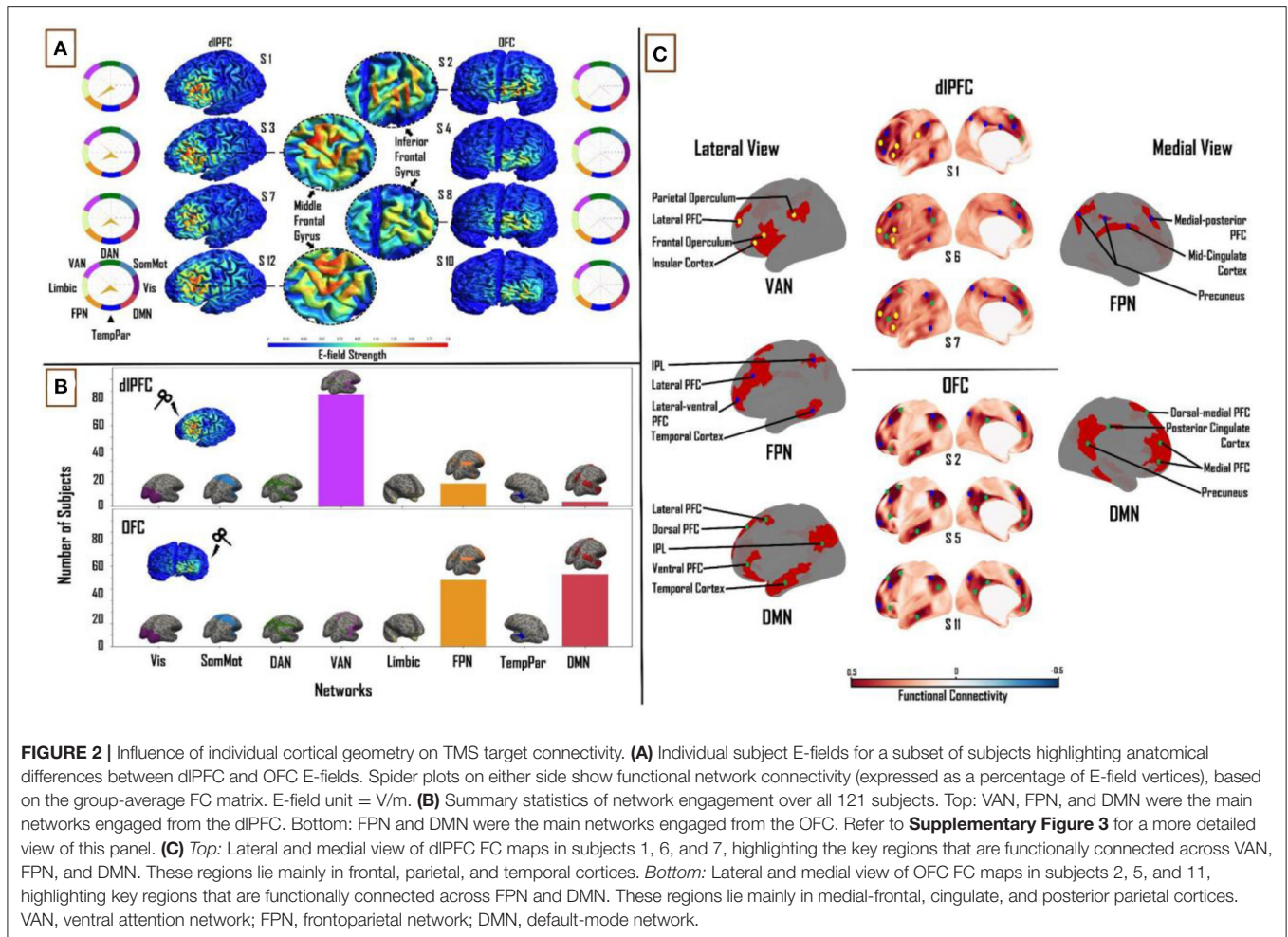
Code and Data Availability

All analyses reported in this paper were conducted on CentOS Linux compute servers running Python 3.7.3, using the standard scientific computing stack and several open-source neuroimaging software tools—principally SimNIBS [E-field simulations; (17)], Nibabel [neuroimaging data I/O; (34)] and Nilearn [neuroimaging data visualizations; (35)]. All code and analysis results are openly available at github.com/griffithslab/HaritaEtAl2022_tms-efield-fc.

RESULTS

Influence of Individual Cortical Geometry on TMS Target Connectivity Patterns: E-field Variability

There was considerable variability in the size of the E-fields across the subject group, as defined by the spatial extent of the thresholded E-field surface maps. At the dlPFC, E-field size ranged from 12 to 112.5 mm² (mean = 54.3 ± 18 mm²). The OFC on the other hand was smaller in terms of overall E-field size, ranging from 3.2 to 60.7 mm² (mean = 16.2 ± 8.5 mm²). The E-field sizes varied to a greater extent for dlPFC stimulation (scalp position F3) than for OFC stimulation (scalp position Fp1; **Figure 2A**). (See Section METHODS for information on the threshold value chosen and on physical dimensions of surface units).



Functional Network Connectivity Based on Subject-Specific E-fields

We analyzed connectivity strength within each subject's E-field maps by comparing maximum FC values (network engagement). A significant main effect of "NETWORK" was found at the dlPFC ($F_{(1,7)} = 1,027.55$, $p < 0.0001$, $\eta^2 = 0.90$) and OFC ($F_{(1,7)} = 1,907.36$, $p < 0.0001$, $\eta^2 = 0.94$). Across all subjects, three networks from the Leo et al. (23) functional network parcellations had maximum FC to vertices in the dlPFC and OFC E-fields. In the dlPFC, the VAN ($38.2 \pm 8\%$), FPN ($27.9 \pm 7\%$), and DMN ($20.3 \pm 6.4\%$) accounted for an average of 86% of the E-field vertices. In the OFC, the FPN ($46.5 \pm 10.3\%$) and DMN ($51.4 \pm 10.3\%$) accounted for 98% of the E-field vertices. The VAN, FPN and DMN were the most engaged networks from the dlPFC across the group (97, 20 and 4 out of 121 subjects, respectively). The DMN was the more engaged network from OFC than the FPN (63 and 58 out of 121 subjects, respectively; **Figure 2B**). Pairwise *t*-tests showed strong interactions between the TMS stimulation sites and the three major functional networks. We found the OFC target region showed greater connectivity to the DMN ($T = 29.2$; $p < 0.0001$) and FPN ($T = 19$; $p < 0.0001$) relative to the dlPFC target region, whereas the dlPFC target

region showed greater connectivity to the VAN ($T = 48.3$; $p < 0.0001$).

Relationship Between TMS Targets and Downstream Brain Regions in Subject-Specific E-fields

After summarizing the overall structure of TMS target connectivity to the rest of the brain in terms of E-field vertex FC to the eight canonical Yeo networks, we examined more closely the spatial topographies of these FC patterns. Specifically, we studied the seed-based FC maps (where the seed is the entire thresholded E-field, and the maps are averaged over vertices within the seed) for each subject and target site, and identified through extensive manual inspection the dominant and consistent sub-patterns within those maps. Specific brain regions in the VAN, FPN, and DMN were highlighted with dlPFC-TMS stimulation. On the lateral cortical surface, key nodes within the VAN included the frontal and parietal opercula, lateral prefrontal cortex (PFC), and insular cortex. The main lateral FPN nodes were the posterior part of the middle and inferior temporal gyri, inferior parietal lobule (IPL), and the lateral-ventral and lateral PFC. Medial FPN nodes included the precuneus, mid-cingulate cortex, and medial-posterior PFC. Within the DMN, we observed the IPL, the lateral and ventral

PFC on the lateral cortical surface; while the dorsal-medial and medial PFC constituted the medial DMN nodes. On the medial surface of the cortex, we observed FPN and DMN nodes, however, there were no specific VAN nodes [Figure 2C (top)]. With regards to the OFC, specific regions in the FPN and DMN were highlighted. Within the FPN, laterally, we observed several of the same nodes noted above, including the lateral-ventral, lateral PFC, and IPL. Medial FPN nodes included the medial-posterior PFC and precuneus. In the DMN, the IPL and lateral PFC were seen once again as key nodes laterally. Medial DMN nodes included the dorsal-medial, medial PFC, and precuneus. DMN nodes specific to the OFC included the dorsal PFC and the anterior portion of the middle and inferior temporal gyri on the lateral cortical surface; and the posterior cingulate cortex (PCC) on the medial cortical surface [Figure 2C (bottom)]. Critically, similar key nodes within different functional networks showed markedly different FC patterns between the two TMS target sites.

Influence of Connectivity Structure on TMS Target Connectivity Patterns

In the previous section, we held the FC matrix fixed, allowing us to characterize inter-subject differences in (putative) TMS target connectivity resulting purely from variation in the head, skull, and brain anatomy and geometry. We now examine the reverse scenario: inter-subject differences in TMS target connectivity due purely to the individualized FC, but using a single fixed E-field map for all subjects.

E-field Variability

The size of the constant E-field at the dlPFC was 31 mm² and at the OFC was 6.3 mm² (Figure 3A).

Functional Network Connectivity Based on Constant E-fields

One-way ANOVA identified a significant main effect of “NETWORK” for both dlPFC ($F_{(1,7)} = 264.37$, $p < 0.0001$, $\eta^2 = 0.69$) and OFC ($F_{(1,7)} = 208.05$, $p < 0.0001$, $\eta^2 = 0.64$). The same three functional networks from the subject-specific analysis were seen to have maximum FC to vertices in the constant E-field across subjects. In the dlPFC, dominant connectivity to the VAN ($30.6 \pm 12.3\%$), FPN ($29 \pm 10.3\%$) and DMN ($21.5 \pm 7.9\%$) together accounted for 81% of E-field vertices. In the OFC, the FPN ($23.4 \pm 13.4\%$) and DMN ($42 \pm 16.3\%$) together accounted for 65% of the E-field vertices. Once again, the VAN, FPN and DMN were the most engaged networks from the dlPFC across the group (61, 39 and 11 out of 121 subjects, respectively). The DMN was more engaged than the FPN in a majority of subjects, from the OFC (78 and 24 out of 121, respectively; Figure 3B). Once again, pairwise t-tests showed strong interactions between the TMS targets and the three major functional networks. We found the OFC target region showed greater connectivity to the DMN ($T = 13.6$; $p < 0.0001$) relative to the dlPFC target region, whereas the dlPFC target region showed greater connectivity to the VAN ($T = 25.2$; $p < 0.0001$) and FPN ($T = 4.1$; $p < 0.0001$).

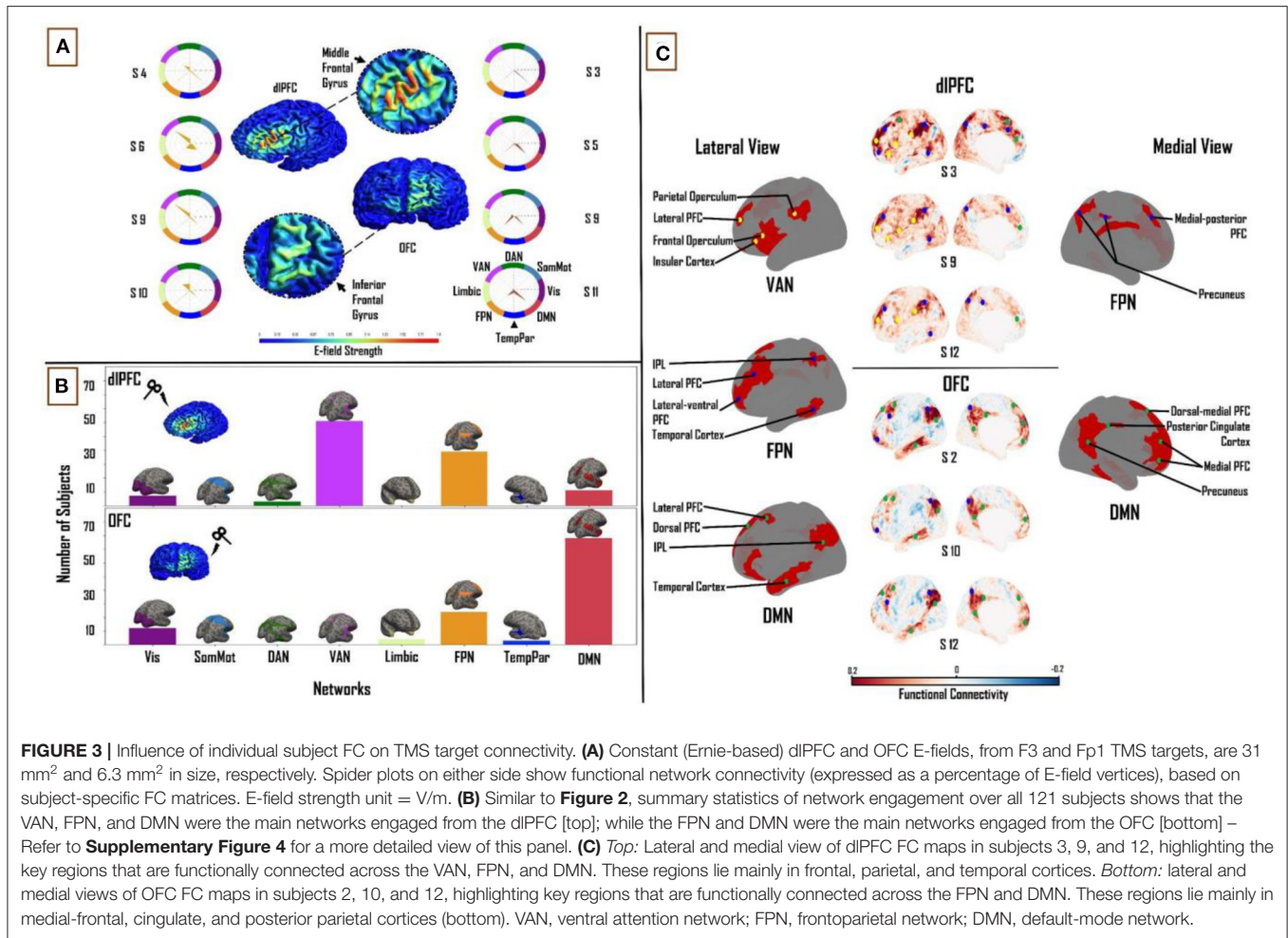
The Relation Between TMS Targets and Downstream Brain Regions in Constant E-fields

Turning again to a detailed inspection of the seed-based FC maps, specific brain regions in the VAN, FPN, and DMN were highlighted with dlPFC-TMS, and within the FPN and DMN in OFC-TMS. Within the VAN, similar to our findings in the previous section, the lateral PFC, frontal and parietal opercula, and the IPL were the key nodes observed on the lateral cortical surface. The lateral FPN nodes included the posterior regions of the middle and inferior temporal gyri, the IPL, and the lateral-ventral and lateral PFC. We noted the precuneus and medial-posterior PFC as the main medial FPN nodes. Key DMN nodes included the lateral PFC and the dorsomedial and medial PFC. Again, as in the previous section, on the medial surface of the cortex, we observed FPN and DMN nodes, but no specific VAN nodes were seen [Figure 3C (top)]. At the OFC, on the lateral left cortical surface, the FPN included some of the same nodes noted above such as the lateral-ventral and lateral PFC and the IPL. The main lateral DMN nodes included the IPL, the anterior portion of the middle and inferior temporal gyri, and the dorsolateral PFC. On the medial left cortical surface, the DMN nodes included the dorsal-medial PFC, medial PFC, precuneus, and PCC [Figure 3C (bottom)]. It is important to clarify here that, while similar brain regions were seen appearing as key nodes within the different functional networks, the FC patterns were markedly different between the two TMS targets and across different subjects.

The Combined Influence of Individual Cortical Geometry and Individual Connectivity Structure on TMS Target Connectivity Patterns

In order to evaluate the similarity of the network engagement in the dlPFC and OFC (when using subject-specific E-fields) between the group average FC matrix and subject-specific FC matrices, we studied the Pearson correlation between the percentage of E-field vertices for the VAN, FPN, and DMN, across all subjects, for these two FC matrix variants. For dlPFC targets, the group average and subject-specific FC matrices showed a higher correlation in the percentage E-field vertices that maximally correlated with the DMN ($r = 0.54$), than the VAN and FPN ($r = 0.19$ and $r = 0.44$, respectively). We found the opposite to be true in the OFC. Here, we observed that there was a higher correlation between the percentage of E-field vertices preferentially correlated with FPN ($r = 0.40$) than with DMN ($r = 0.23$), when comparing group average and subject-specific FC matrices.

Similarly, to determine the similarity of the network engagement in the dlPFC and OFC (when using subject-specific FC matrices) between the fixed (“Ernie”) E-field and subject-specific E-field, we looked at the Pearson correlation between the percentage of E-field vertices, for the VAN, FPN, and DMN, across all subjects, for the two E-field variants. In the dlPFC, the fixed and subject-specific E-fields showed a higher degree of correlation in the proportion of vertices in each subject’s specific FC matrix maximally targeting the VAN ($r = 0.80$), followed by the FPN ($r = 0.63$), and lastly the ($r = 0.56$). In the OFC, we



noticed the reverse to be true. The fixed and subject-specific E-field showed a higher correlation in the proportion of vertices correlated with the DMN ($r = 0.4$), than with the FPN ($r = 0.2$). A comparison of the differences in patterns of FC between the fixed E-field and the subject-specific E-field can be found in **Figure 4A**. Taken together, these analyses indicate that the average E-field and group-average FC data are able to predict which networks are targeted, for some networks, but cannot necessarily tell the degree to which each individual network is specifically targeted across subjects.

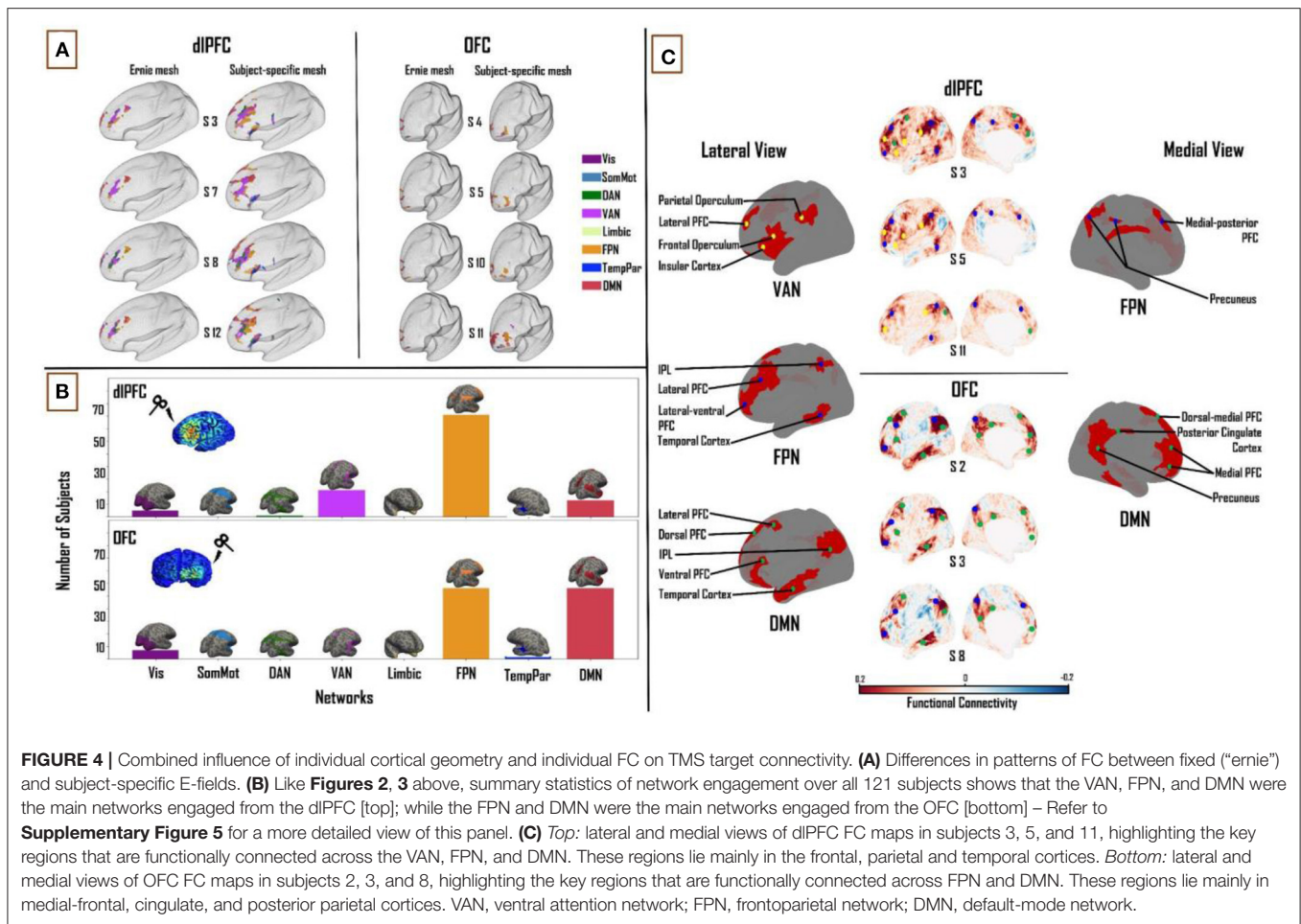
Functional Network Connectivity Based on Subject-Specific E-fields and Subject-Specific Functional Connectivity Matrices

Again, one-way ANOVA showed a significant main effect of “NETWORK” for dIPFC ($F_{(1,7)} = 267.71, p < 0.0001, \eta^2 = 0.69$) and OFC ($F_{(1,7)} = 326.36, p < 0.0001, \eta^2 = 0.73$). In the dIPFC, VAN ($22.2 \pm 9.7\%$), FPN ($34.6 \pm 10.2\%$) and DMN ($18.4 \pm 8.1\%$) were seen to account for 75% of the E-field vertices. FPN ($38.1 \pm 12.9\%$) and DMN ($37.8 \pm 16.5\%$) accounted for 76% of the E-field vertices in the OFC. Unlike the previous two sections, the FPN was the most engaged network from the dIPFC, followed by

the VAN and DMN across the group (81, 21 and 13 out of 121 subjects, respectively). The DMN and FPN were equally engaged from the OFC (56 subjects each out of 121; **Figure 4B**). Similar to the previous sections, pairwise t-tests showed strong interactions between the TMS target areas and the three major networks. We found the OFC target region showed greater connectivity to the DMN ($T = 14.2; p < 0.0001$) and FPN ($T = 2.6; p < 0.01$) relative to the dIPFC target region, whereas the dIPFC target region showed greater connectivity to the VAN ($T = 23.3; p < 0.0001$).

The Relation Between TMS Targets and Downstream Brain Regions

At the dIPFC, on the lateral left cortical surface, the IPL, frontal and parietal opercula, and lateral PFC were the major VAN nodes. Lateral FPN nodes included the IPL, the lateral-ventral and lateral PFC, and the posterior region of the middle and inferior temporal gyri. Medially, the FPN nodes consisted of the medial-posterior PFC and the precuneus. The lateral DMN nodes included the lateral PFC, ventral PFC, and IPL. Medially, the DMN nodes included the dorsal-medial and medial PFC. Once again, similar to the previous sections, no VAN



nodes were observed on the medial cortical surface [**Figure 4C** (top)]. At the OFC, on the lateral cortical surface, the FPN nodes included the IPL, lateral-ventral, and lateral PFC. Medial FPN nodes included the precuneus and medial-posterior PFC. Within the DMN, the IPL, lateral and dorsal PFCs, and the anterior region of the middle and inferior temporal gyri were noted as the main lateral nodes. Medially, the precuneus, PCC, dorsal-medial, and medial PFC made up the DMN nodes [**Figure 4C** (bottom)].

DISCUSSION

In this study, we sought to characterize comprehensively two major therapeutic TMS target sites, the dIPFC and the OFC, in terms of (a) their patterns of FC to other regions and canonical brain networks, and (b) the level and sources of inter-subject variability in those connectivity patterns, using a combination of E-field modeling and analyses of resting-state fMRI data in a group of healthy subjects. With respect to the first of these, our chief conclusion was that three major functional networks were targeted across the dIPFC and OFC: VAN, FPN, and DMN in the dIPFC, and FPN and

DMN in the OFC. Furthermore, while these major networks consistently appeared across all subjects, the relative connectivity strengths between the networks, as well as the downstream nodes within each network, varied considerably on a subject-wise basis. This is consistent with previous observations in both animals (36) and humans (37). With respect to the question of the level and sources of variability, our approach was to separate, and study both independently and in combination, the effects of variability in skull anatomy and cortical geometry (as encapsulated in subject-specific E-field maps), and of variability in subject-specific FC maps. These analyses showed that the average E-field and group-average FC data are able to predict which networks are targeted, for some networks, but cannot necessarily tell the degree to which each individual network is specifically targeted across subjects. In the following, we discuss the key components of these findings, their interpretation in relation to previous work, and highlight important caveats and limitations.

Connectivity of TMS Targets

Regions showing strong FC with TMS targets give us some insight into the potential functional effects of TMS stimulation.

The results of our study revealed the VAN, FPN, and DMN as the major functional networks targeted by dlPFC TMS, and the FPN and DMN as the major networks targeted by OFC TMS. Specific network nodes within each of these networks were observed. Some network nodes such as the lateral PFC (VAN, FPN, and DMN) and precuneus (FPN and DMN) were seen across all subjects and in multiple networks. On the other hand, certain networks and nodes were specific to dlPFC TMS or OFC TMS. For example, the connectivity to the VAN is seen in dlPFC TMS, but not in OFC TMS. At the level of individual network nodes, the PCC is a DMN-specific node in E-field FC patterns for OFC TMS targets, but not dlPFC TMS targets. Furthermore, while many similar nodes occur across these networks in multiple subjects, the overall pattern of FC observed varies from subject to subject. The relevance and important functions of the three major functional networks highlighted in these results (FPN, DMN, and VAN) are outlined below.

The FPN is a system implicated in cognitive control for regulating goal-driven behavior. This network is believed to play a key role in problem-solving, as well as actively preserving and editing the information stored in working memory (38). The DMN is active during resting wakefulness when an individual is not actively engaged with external stimuli (39). The DMN is also involved in ruminative processes, specifically with thoughts concerning oneself, their past or future events (40). The VAN, sometimes called the salience network, keeps track of salient events (triggered by sensory stimuli) and plays a role in response inhibition or selection (41). The VAN is crucial for spontaneous cognitive control, where it helps switch between the DMN's ruminative/self-reflective functions to the FPN's task-based/externally driven functions (41, 42). Neuroimaging studies have shown that the heterogeneous nature of MDD and its subtypes may emerge as a result of unique patterns of disruption in these networks' dynamics (11). Indeed, multiple research groups have begun to utilize abnormal FC patterns to characterize MDD subtypes (43), showing how differences in spontaneous dynamics might potentially lead to different clinical outcomes (7). In line with this evidence, our results suggest that a connectivity-based targeting strategy for optimizing network engagement on a per-subject basis may be beneficial for optimizing clinical responses.

Implications for rTMS Therapy

A systematic review of 25 neuroimaging studies of MDD summarized that hypoconnectivity occurs within the FPN and VAN, while regions that were a part of the DMN exhibited hyperconnectivity (44). There are multiple inhibitory and excitatory rTMS protocols used for inducing region-specific changes in neural activity. Excitatory paradigms include intermittent theta-burst stimulation (iTBS) and high-frequency (10–20 Hz) rTMS, whereas prevalent inhibitory paradigms are continuous theta-burst stimulation (cTBS) and low frequency (~1 Hz) rTMS (4, 45). The implications from our results may further enhance rTMS targeting practices by informing not only regions but also the type of paradigm to use as well. In our study,

a majority of subjects had a higher network engagement with the FPN or VAN than DMN, in the dlPFC [Figure 4B (top)]. Therefore, one way of understanding the positive therapeutic effects of applying iTBS or high-frequency rTMS at the dlPFC in MDD patients may be that this intervention could result in an excitation - and perhaps renormalization - of the VAN and FPN networks, which show hypoconnectivity in MDD (44). At the OFC, our results show a similar network engagement between the DMN and the FPN [Figure 4B (bottom)]. However, the DMN is engaged more from the OFC than from the dlPFC. Thus, in this case, applying cTBS or low-frequency rTMS may be expected to inhibit the DMN, and again potentially achieve a renormalization of DMN hyperconnectivity in MDD. However, we would like to note here that due to similar network engagement of the FPN and DMN from the OFC, the extent to which one is engaged over the other depends on that subject's specific FC. A more DMN-centric target could be the dmPFC (4) as the DMN has more nodes on the medial cortical surface. Targeting specific networks with unique rTMS paradigms in this way may alleviate depressive symptoms more efficiently. In the future, this line of research may be further explored to identify which networks are affected in a given patient, and selectively target them, thereby potentially personalizing rTMS therapy for individuals with MDD.

Functional Connectivity Variability

We calculated the Pearson correlation coefficient between the percentage of E-field vertices for the VAN, FPN, and DMN, across all subjects, for the group average FC matrix and the subject-specific FC matrix. The group average FC matrices were able to predict inter-individual differences in how networks were targeted from the dlPFC and OFC to a certain extent. In the dlPFC, we observed that the 1,003-subject HCP average FC matrix was able to predict what DMN connectivity would be with the subject-specific FC matrices ($r = 0.54$) better than with the VAN ($r = 0.19$) and FPN connectivity ($r = 0.44$). However, this observation was reversed in the OFC. Here, the average FC matrix was able to predict what FPN connectivity would be with subject-specific FC matrices ($r = 0.40$) better than with the DMN ($r = 0.23$). One explanation for this finding is that DMN has a more consistent spatial pattern across subjects than the VAN or FPN, such that subject-level and group-level patterns are relatively more similar than for other networks. However, this line of reasoning does not explain why a pattern reversal occurs at the OFC. In summary, our results confirm the general intuition that using an average FC matrix provides a gross estimate of what the targeted networks might be, but precise targeting requires each subject's specific FC data.

E-field Variability

We observed the mean subject-specific thresholded E-field size to be 54.3 and 16.2 mm², in the dlPFC and OFC, respectively. However, the E-field size varied considerably across subjects, with a standard deviation of ± 18 mm² in the dlPFC and ± 8 mm² in the OFC. This high intersubject variability of dlPFC and OFC E-fields can be attributed to variability in subject-specific cortical geometry. Consistent with this, the boundaries between the five main tissue types have been shown to affect E-field distributions.

These include the skin, skull, CSF, white matter, and gray matter (20), and are highly variable across subjects. Furthermore, this E-field variability had a knock-on effect on variability in the connectivity of the dlPFC and OFC stimulation targets to downstream functional networks. In the dlPFC, the normative template E-field (from the “ernie” brain) and subject-specific E-fields showed the highest network engagement correlation with the VAN ($r = 0.80$), followed by the and FPN ($r = 0.63$) and then the DMN ($r = 0.56$), in each subject’s specific FC matrix. In the OFC, the opposite was found to be true. The normative template E-field and subject-specific E-field showed a higher network engagement correlation with the DMN ($r = 0.4$), than the FPN ($r = 0.2$). A potential reason for this observation is the large difference in size between the template E-field and the subject-specific E-fields. In the dlPFC, the subject-specific E-fields are nearly twice as large (mean = 54.3 mm²) as the template E-field (31 mm²). The difference is greater in the OFC, with the subject-specific E-fields (mean = 16.2 mm²) being over two and half times the size of the template E-field (6.3 mm²). The additional vertices in each subjects’ specific E-field tend to target the VAN and FPN in the dlPFC, as the E-field vertices here are predominantly present on the ventral/lateral surface of the prefrontal cortex. The DMN, being more medially located overall, therefore has lower connectivity to dlPFC when the template E-field is used than when subject-specific E-fields are used [Figure 4A (left)]. Furthermore, this line of reasoning can be extended to account for the pattern reversal observed in the OFC, where the template E-field does not account for the additional vertices in the subject-specific E-fields which are spread more laterally, targeting the FPN (Figure 4A (right)), and hence shows a pattern targeting the DMN but not the FPN.

Caveats and Limitations

While the results of this study are promising, there are some important caveats and limitations to highlight.

One important limitation is the fact that we only use the left hemisphere to study TMS target connectivity. The reason for this choice was in part practical (simplifying surface-based analysis), but also reflected the fact that as a rule, we expect FC patterns to the two TMS target zones to be dominated by intrahemispheric connections, with the obvious exception of the contralateral homolog (i.e., right dlPFC and right OFC). By using FC data from only one hemisphere, we are therefore potentially missing some important differences between subjects and TMS targets in their connectivity to the contralateral homologs. Moreover, our choice was also driven by common practice in clinical settings which use the left hemisphere as a target for rTMS treatments. However, given that our focus here is on patterns of FC to distal cortical regions that are outside of either the primary target area or its hemispheric homolog, we feel this approach is justified.

Another important limitation is the E-field threshold and its effect on resultant FC calculations. In this study, the E-field threshold was set to 0.9 V/m, which is slightly lower than that used by Romero et al. (28). Our justification for this choice is that higher thresholds (i.e., above 0.9 V/m) shrink the E-field sizes, especially in the OFC, and hamper FC calculations. The problem remains however that in the field of TMS more broadly,

it is not yet clear what a “correct” E-field threshold should be. Thus, we explored the effects of using a range of E-field values and these results are detailed in the **Supplementary Information** section. Often the “correct” E-field threshold is conceived as the minimum induced current necessary to depolarize neuronal membranes and cause them to fire. Subthreshold effects (i.e., ones not resulting from action potential induction at the primary stimulation site) may nevertheless potentially have an important role in TMS responses; for example by facilitating the occurrence and frequency of suprathreshold events. Spatially, the question of E-field thresholding relates quite closely to the question of E-Field size and extent (since high thresholds usually “trim” the edges of activated areas, eliminating vertices around the penumbra first).

A further, related, limitation is that interpretation of our results, and those from related work [e.g., (21)] rests heavily on the notion that FC can serve as a reliable indicator of which downstream brain regions, distal to the TMS target site, would themselves be “activated,” or otherwise affected, by TMS administration. In defense of this principle, multiple studies have shown experimentally that neuronal activation as a result of TMS is not limited to the cortical circuits closest to the scalp (46–49). These studies show that initial local neuronal activation spreads across cortical and subcortical regions to neighboring and distant parts of the brain. In other words, it appears to be impossible to stimulate a single region of the brain with TMS without affecting a large number of downstream network nodes. While further studies are required to decipher the precise pathways taken to activate these downstream nodes, FC maps offer a plausible proxy for assessing which networks are being engaged for a given TMS target region.

Importantly, the subjects chosen for this study are from a normative, healthy sample (from the HCP database). However, MDD patients may have different/altered connectivity patterns that the healthy subject patterns may not be representative of. While previous research has looked at connectivity-based targeting in MDD patients with promising results (50), a full-fledged clinical trial evaluating this method is yet to be undertaken (8).

One potential improvement to the methodology used here that may be considered for future work is to evaluate alternative TMS coil options. Here, we have chosen to use the Magstim 70 mm Figure-8 coil to run our TMS simulations in SimNIBS. Used in both clinical and research settings, it has been shown that Figure-8 coils allow for a more focused stimulation of the target site (51) than other design options. We used the Figure-8 coil type to run our simulations for both the dlPFC and OFC. However, the thresholded E-field size difference between these two TMS targets in our analyses is likely due mainly to their anatomical locations, and distance from the stimulating coil. The dlPFC is located at the frontal lobe and lies on the lateral and dorsal surface of the medial convexity, fairly close to the scalp surface. The OFC, on the other hand, is a large gray matter shelf located on the ventral surface of the frontal lobes, above the orbit of the skull. As a result, a large portion of the OFC is not accessible *via* the Fp1 electrode position on the scalp (which is more frontal in location than ventral). Thus, a typical Figure-8 coil cannot target the OFC as effectively as it can the dlPFC, owing to the inconsistency of the

targeting surface. To address this issue, alternate coil designs have been proposed, such as crown-shaped coils, C-shaped coils (52), and H-shaped coils (53), which have been developed to target deeper cortical regions. It will be valuable to analyze the resulting E-fields produced by these coils with our current methodology, to better establish the effects of TMS with all potentially available coil configurations on novel treatment sites, such as the ventral OFC and regions of the medial PFC.

Finally, we note that in addition to the network properties explored in the present work, we believe it is also important to consider the following supplementary network properties as they are likely critical to improving our understanding of the precise rTMS mechanism of action. Local excitatory/inhibitory (E/I) ratios mainly concern the action of the neurotransmitter γ -aminobutyric acid (GABA). Previous research has shown using short-interval intracortical inhibition (SICI), which is known to be strongly driven by GABAA synaptic activity, that the excitatory effect of 10 Hz rTMS is likely due to reduced overall inhibition in the cortex due to reduced GABAA activity (54, 55). Similarly, TMS-EEG studies have shown that excitatory rTMS alters early (50 and 100 ms) TMS evoked potential (TEP) components (56), which in turn have been demonstrated in pharmacological studies to reflect GABAA and GABAB receptor activity (57). Future work should aim to integrate more comprehensively the neuroanatomical network-based approach taken in the present study and these insights into physiological effects of TMS.

CONCLUSIONS AND FUTURE DIRECTIONS

We have presented data characterizing the FC patterns of canonical therapeutic TMS targets and the key dimensions of their variability across subjects. Our results show that the VAN, FPN, and DMN are the major functional networks targeted by dlPFC TMS, and the FPN and DMN are the major networks targeted by OFC TMS. These results provide important insights into the functional neuroanatomical effects of clinical TMS stimulation protocols. Importantly, our results validate the general intuition that using a normative group-averaged FC matrix provides only a coarse estimate of what the targeted networks might be, and precise targeting requires each subject's specific FC data.

Our hope is that these insights prove useful as part of the broader effort by the psychiatry, neurology, and neuroimaging communities to help improve and refine TMS therapy, through a better understanding of the technology and its neurophysiological effects. Further work shall be needed to evaluate the predictive and clinical utility of the TMS target fMRI FC profiles, through both prospective and retrospective clinical neuroimaging studies in MDD patients. Progress on the neurobiological question of what are the network-level effects of TMS stimulation, however, necessitates an integrative approach combining various neuroimaging and physiological modalities, and various quantitative techniques. In particular,

characterization of the structural connectivity between TMS targets and their downstream networks using diffusion-weighted MRI tractography analyses, which can serve as a useful proxy for axonal connectivity between various brain regions, shall be an important area of investigation that should complement the results reported in the present study. How do target region connectivity profiles from tractography connectivity compare to their FC analogs? How should discrepancies and convergences between structure and function be interpreted in relation to expected TMS effects? Another important question we hope to answer in the future is how using different locations with the same target regions affects downstream FC. For example, both the F3 and F5 electrode locations fall within the dlPFC. It would be interesting to study the differences in network engagement in this situation. Ultimately the best-known general strategy for reconciling such questions (and one that we are currently pursuing intensively) is to develop validated and predictively accurate computational models of brain stimulation responses, that include relevant biological detail but are also sufficiently scalable to allow whole-brain activity simulations. In future work, our aim is to use mechanistic modeling approaches to formalize and test hypotheses around synaptic-, local circuit-, and network-level mechanisms in brains receiving noninvasive stimulation, and to use the insights obtained to help improve the efficacy of TMS in the clinic.

DATA AVAILABILITY STATEMENT

The original contributions presented in the study are included in the article/**Supplementary Material**, further inquiries can be directed to the corresponding author.

AUTHOR CONTRIBUTIONS

SH: conceptualization, methodology, formal analysis, writing—original draft, writing—review and editing, and visualization. JG: conceptualization, methodology, writing—review and editing, supervision, and funding acquisition. DM: writing—review and editing, visualization. FM: writing—review and editing. All authors contributed to the article and approved the submitted version.

FUNDING

We are grateful to the Krembil Foundation, CAMH Discovery Fund, and Labatt Family Network for the generous funding support that has made this research possible.

SUPPLEMENTARY MATERIAL

The Supplementary Material for this article can be found online at: <https://www.frontiersin.org/articles/10.3389/fpsy.2022.902089/full#supplementary-material>

REFERENCES

- MacQueen G, Santaguida P, Keshavarz H, Jaworska N, Levine M, Beyene J, et al. Systematic review of clinical practice guidelines for failed antidepressant treatment response in major depressive disorder, dysthymia, and subthreshold depression in adults. *Can J Psychiatry*. (2017) 62:11–23. doi: 10.1177/0706743716664885
- Souery D, Amsterdam J, de Montigny C, Lecrubier Y, Montgomery S, Lipp O, et al. Treatment resistant depression: methodological overview and operational criteria. *Eur Neuropsychopharmacol*. (1999) 9:83–91. doi: 10.1016/S0924-977X(98)00004-2
- Nestor SM, Blumberger DM. Mapping symptom clusters to circuits: toward personalizing TMS targets to improve treatment outcomes in depression. *Am J Psychiatry*. (2020) 177:373–5. doi: 10.1176/appi.ajp.2020.20030271
- Downar J, Daskalakis ZJ. New targets for rTMS in depression: a review of convergent evidence. *Brain Stimul*. (2013) 6:231–40. doi: 10.1016/j.brs.2012.08.006
- Fox MD, Liu H, Pascual-Leone A. Identification of reproducible individualized targets for treatment of depression with TMS based on intrinsic connectivity. *Neuroimage*. (2013) 66:151–60. doi: 10.1016/j.neuroimage.2012.10.082
- Drysdale AT, Grosenick L, Downar J, Dunlop K, Mansouri F, Meng Y, et al. Resting-state connectivity biomarkers define neurophysiological subtypes of depression. *Nat Med*. (2017) 23:28–38. doi: 10.1038/nm.4246
- Fox MD, Buckner RL, White MP, Greicius MD, Pascual-Leone A. Efficacy of transcranial magnetic stimulation targets for depression is related to intrinsic functional connectivity with the subgenual cingulate. *Biol Psychiatry*. (2012) 72:595–603. doi: 10.1016/j.biopsych.2012.04.028
- Cash RFH, Weigand A, Zalesky A, Siddiqi SH, Downar J, Fitzgerald PB, et al. Using brain imaging to improve spatial targeting of transcranial magnetic stimulation for depression. *Biol Psychiatry*. (2020) 90:689–700. doi: 10.1016/j.biopsych.2020.05.033
- Tik M, Hoffmann A, Sladky R, Tomova L, Hummer A, Navarro de Lara L, et al. Towards understanding rTMS mechanism of action: stimulation of the DLPFC causes network-specific increase in functional connectivity. *Neuroimage*. (2017) 162:289–96. doi: 10.1016/j.neuroimage.2017.09.022
- Fitzgerald PB, Hoy KE, Anderson RJ, Daskalakis ZJ. A study of the pattern of response to rTMS treatment in depression. *Depress Anxiety*. (2016) 33:746–53. doi: 10.1002/da.22503
- Feffer K, Fettes P, Giacobbe P, Daskalakis ZJ, Blumberger DM, Downar J. 1Hz rTMS of the right orbitofrontal cortex for major depression: safety, tolerability and clinical outcomes. *Eur Neuropsychopharmacol*. (2018) 28:109–17. doi: 10.1016/j.euroneuro.2017.11.011
- Zald DH, McHugo M, Ray KL, Glahn DC, Eickhoff SB, Laird AR. Meta-analytic connectivity modeling reveals differential functional connectivity of the medial and lateral orbitofrontal cortex. *Cereb Cortex*. (2014) 24:232–48. doi: 10.1093/cercor/bhs308
- Kringelbach ML. The human orbitofrontal cortex: linking reward to hedonic experience. *Nat Rev Neurosci*. (2005) 6:691–702. doi: 10.1038/nrn1747
- Boorman ED, Rushworth MF, Behrens TE. Ventromedial prefrontal and anterior cingulate cortex adopt choice and default reference frames during sequential multi-alternative choice. *J Neurosci*. (2013) 33:2242–53. doi: 10.1523/JNEUROSCI.3022-12.2013
- Rolls ET. The orbitofrontal cortex and emotion in health and disease, including depression. *Neuropsychologia*. (2019) 128:14–43. doi: 10.1016/j.neuropsychologia.2017.09.021
- Kumar S, Singh S, Chadda RK, Verma R, Kumar N. The effect of low-frequency repetitive transcranial magnetic stimulation at orbitofrontal cortex in the treatment of patients with medication-refractory obsessive-compulsive disorder: a retrospective open study. *J ECT*. (2018) 34:e16–9. doi: 10.1097/YCT.0000000000000462
- Thielscher A, Antunes A, Saturnino GB. Field modeling for transcranial magnetic stimulation: a useful tool to understand the physiological effects of TMS? In: *2015 37th Annual International Conference of the IEEE Engineering in Medicine and Biology Society (EMBC)* (Milan). (2015), p. 222–5. doi: 10.1109/EMBC.2015.7318340
- Weise K, Numssen O, Thielscher A, Hartwigsen G, Knösche TR. A novel approach to localize cortical TMS effects. *Neuroimage*. (2020) 209:116486. doi: 10.1016/j.neuroimage.2019.116486
- Opitz A, Windhoff M, Heidemann RM, Turner R, Thielscher A. How the brain tissue shapes the electric field induced by transcranial magnetic stimulation. *Neuroimage*. (2011) 58:849–59. doi: 10.1016/j.neuroimage.2011.06.069
- Thielscher A, Opitz A, Windhoff M. Impact of the gyral geometry on the electric field induced by transcranial magnetic stimulation. *Neuroimage*. (2011) 54:234–43. doi: 10.1016/j.neuroimage.2010.07.061
- Opitz A, Fox MD, Craddock RC, Colcombe S, Milham MP. An integrated framework for targeting functional networks via transcranial magnetic stimulation. *Neuroimage*. (2016) 127:86–96. doi: 10.1016/j.neuroimage.2015.11.040
- Vila-Rodriguez F, Frangou S. Individualized functional targeting for rTMS: a powerful idea whose time has come? *Hum Brain Mapp*. (2021) 42:4079–80. doi: 10.1002/hbm.25543
- Yeo BTT, Krienen FM, Sepulcre J, Sabuncu MR, Lashkari D, Hollinshead M, et al. The organization of the human cerebral cortex estimated by intrinsic functional connectivity. *J Neurophysiol*. (2011) 106:1125–65. doi: 10.1152/jn.00338.2011
- Fettes PW. *Orbitofrontal cortex repetitive transcranial magnetic stimulation for the treatment of major depressive disorder*. (2020). Available online at: <https://tspace.library.utoronto.ca/handle/1807/101082> (accessed June 7, 2021).
- George MS, Wassermann EM, Williams WA, Callahan A, Ketter TA, Basser P, et al. Daily repetitive transcranial magnetic stimulation (rTMS) improves mood in depression. *Neuroreport*. (1995) 6:1853–6. doi: 10.1097/00001756-199510020-00008
- Pascual-Leone A, Rubio B, Pallardó F, Catalá MD. Rapid-rate transcranial magnetic stimulation of left dorsolateral prefrontal cortex in drug-resistant depression. *Lancet*. (1996) 348:233–7. doi: 10.1016/S0140-6736(96)01219-6
- Janssen AM, Oostendorp TF, Stegeman DF. The coil orientation dependency of the electric field induced by TMS for M1 and other brain areas. *J Neuroeng Rehabil*. (2015) 12:47. doi: 10.1186/s12984-015-0036-2
- Romero MC, Davare M, Armendariz M, Janssen P. Neural effects of transcranial magnetic stimulation at the single-cell level. *Nat Commun*. (2019) 10:2642. doi: 10.1038/s41467-019-10638-7
- Van Essen DC, Ugurbil K, Auerbach E, Barch D, Behrens TEJ, Bucholz R, et al. The Human Connectome Project: a data acquisition perspective. *Neuroimage*. (2012) 62:2222–31. doi: 10.1016/j.neuroimage.2012.02.018
- Van Essen DC, Smith SM, Barch DM, Behrens TEJ, Yacoub E, Ugurbil K, et al. The WU-Minn Human Connectome Project: an overview. *Neuroimage*. (2013) 80:62–79. doi: 10.1016/j.neuroimage.2013.05.041
- Ugurbil K, Xu J, Auerbach EJ, Moeller S, Vu AT, Duarte-Carvajalino JM, et al. Pushing spatial and temporal resolution for functional and diffusion MRI in the Human Connectome Project. *Neuroimage*. (2013) 80:80–104. doi: 10.1016/j.neuroimage.2013.05.012
- Glasser MF, Sotiropoulos SN, Wilson JA, Coalson TS, Fischl B, Andersson JL, et al. The minimal preprocessing pipelines for the Human Connectome Project. *Neuroimage*. (2013) 80:105–24. doi: 10.1016/j.neuroimage.2013.04.127
- Schaefer A, Kong R, Gordon EM, Laumann TO, Zuo X-N, Holmes AJ, et al. Local-global parcellation of the human cerebral cortex from intrinsic functional connectivity MRI. *Cereb Cortex*. (2018) 28:3095–114. doi: 10.1093/cercor/bhx179
- Brett M, Markiewicz CJ, Hanke M, Côté M-A, Cipollini B, McCarthy P, et al. nipy/nibabel: 3.2.1. *Zenodo*. (2020). doi: 10.5281/zenodo.591597
- Abraham A, Pedregosa F, Eickenberg M, Gervais P, Mueller A, Kossaifi J, et al. Machine learning for neuroimaging with scikit-learn. *Front Neuroinform*. (2014) 8:14. doi: 10.3389/fninf.2014.00014
- Bergmann E, Gofman X, Kavushansky A, Kahn I. Individual variability in functional connectivity architecture of the mouse brain. *Commun Biol*. (2020) 3:738. doi: 10.1038/s42003-020-01472-5
- Mueller S, Wang D, Fox MD, Yeo BTT, Sepulcre J, Sabuncu MR, et al. Individual variability in functional connectivity architecture of the human brain. *Neuron*. (2013) 77:586–95. doi: 10.1016/j.neuron.2012.12.028
- Uddin LQ, Yeo BTT, Spreng RN. Towards a universal taxonomy of macro-scale functional human brain networks. *Brain Topogr*. (2019) 32:926–42. doi: 10.1007/s10548-019-00744-6
- Fox MD, Snyder AZ, Vincent JL, Corbetta M, Van Essen DC, Raichle ME. The human brain is intrinsically organized into dynamic, anticorrelated

- functional networks. *Proc Natl Acad Sci USA*. (2005) 102:9673–8. doi: 10.1073/pnas.0504136102
40. Andrews-Hanna JR. The brain's default network and its adaptive role in internal mentation. *Neuroscientist*. (2012) 18:251–70. doi: 10.1177/1073858411403316
 41. Menon V, Uddin LQ. Saliency, switching, attention and control: a network model of insula function. *Brain Struct Funct*. (2010) 214:655–67. doi: 10.1007/s00429-010-0262-0
 42. Menon V. Large-scale brain networks and psychopathology: a unifying triple network model. *Trends Cogn Sci*. (2011) 15:483–506. doi: 10.1016/j.tics.2011.08.003
 43. Peng D-H, Shen T, Zhang J, Huang J, Liu J, Liu S-Y, et al. Abnormal functional connectivity with mood regulating circuit in unmedicated individual with major depression: a resting-state functional magnetic resonance study. *Chin Med J*. (2012) 125:3701–6. doi: 10.3760/cma.j.issn.0366-6999.2012.20.01
 44. Kaiser RH, Andrews-Hanna JR, Wager TD, Pizzagalli DA. Large-Scale Network dysfunction in major depressive disorder: a meta-analysis of resting-state functional connectivity. *JAMA Psychiatry*. (2015) 72:603–11. doi: 10.1001/jamapsychiatry.2015.0071
 45. Huang Y-Z, Edwards MJ, Rouin E, Bhatia KP, Rothwell JC. Theta burst stimulation of the human motor cortex. *Neuron*. (2005) 45:201–6. doi: 10.1016/j.neuron.2004.12.033
 46. Siebner HR, Bergmann TO, Bestmann S, Massimini M, Johansen-Berg H, Mochizuki H, et al. Consensus paper: combining transcranial stimulation with neuroimaging. *Brain Stimul*. (2009) 2:58–80. doi: 10.1016/j.brs.2008.11.002
 47. Solomon-Harris LM, Rafique SA, Steeves JKE. Consecutive TMS-fMRI reveals remote effects of neural noise to the “occipital face area”. *Brain Res*. (2016) 1650:134–41. doi: 10.1016/j.brainres.2016.08.043
 48. Hawco C, Voineskos AN, Steeves JKE, Dickie EW, Viviano JD, Downar J, et al. Spread of activity following TMS is related to intrinsic resting connectivity to the salience network: a concurrent TMS-fMRI study. *Cortex*. (2018) 108:160–72. doi: 10.1016/j.cortex.2018.07.010
 49. Bergmann TO, Varatheeswaran R, Hanlon CA, Madsen KH, Thielscher A, Siebner HR. Concurrent TMS-fMRI for causal network perturbation and proof of target engagement. *Neuroimage*. (2021) 237:118093. doi: 10.1016/j.neuroimage.2021.118093
 50. Weigand A, Horn A, Caballero R, Cooke D, Stern AP, Taylor SF, et al. Prospective validation that subgenual connectivity predicts antidepressant efficacy of transcranial magnetic stimulation sites. *Biol Psychiatry*. (2018) 84:28–37. doi: 10.1016/j.biopsych.2017.10.028
 51. Thielscher A, Kammer T. Electric field properties of two commercial figure-8 coils in TMS: calculation of focality and efficiency. *Clin Neurophysiol*. (2004) 115:1697–708. doi: 10.1016/j.clinph.2004.02.019
 52. Deng Z-D, Peterchev AV, Lisanby SH. Coil design considerations for deep-brain transcranial magnetic stimulation (dTMS). *Conf Proc IEEE Eng Med Biol Soc*. (2008) 2008:5675–9. doi: 10.1109/IEMBS.2008.4650502
 53. Levkovitz Y, Harel EV, Roth Y, Braw Y, Most D, Katz LN, et al. Deep transcranial magnetic stimulation over the prefrontal cortex: evaluation of antidepressant and cognitive effects in depressive patients. *Brain Stimul*. (2009) 2:188–200. doi: 10.1016/j.brs.2009.08.002
 54. Pascual-Leone A, Tormos JM, Keenan J, Tarazona F, Cañete C, Catalá MD. Study and modulation of human cortical excitability with transcranial magnetic stimulation. *J Clin Neurophysiol*. (1998) 15:333–43. doi: 10.1097/00004691-199807000-00005
 55. Fitzgerald PB, Daskalakis ZJ. The mechanism of action of rTMS. In: Fitzgerald PB, Daskalakis ZJ, editors. *rTMS Treatment for Depression: A Practical Guide*. Cham: Springer International Publishing (2022), p. 13–28. doi: 10.1007/978-3-030-91519-3_3
 56. Voineskos D, Blumberger DM, Rogasch NC, Zomorrodi R, Farzan F, Foussias G, et al. Neurophysiological effects of repetitive transcranial magnetic stimulation (rTMS) in treatment resistant depression. *Clin Neurophysiol*. (2021) 132:2306–16. doi: 10.1016/j.clinph.2021.05.008
 57. Premoli I, Castellanos N, Rivolta D, Belardinelli P, Bajo R, Zipser C, et al. TMS-EEG signatures of GABAergic neurotransmission in the human cortex. *J Neurosci*. (2014) 34:5603–12. doi: 10.1523/JNEUROSCI.5089-13.2014

Conflict of Interest: The authors declare that the research was conducted in the absence of any commercial or financial relationships that could be construed as a potential conflict of interest.

Publisher's Note: All claims expressed in this article are solely those of the authors and do not necessarily represent those of their affiliated organizations, or those of the publisher, the editors and the reviewers. Any product that may be evaluated in this article, or claim that may be made by its manufacturer, is not guaranteed or endorsed by the publisher.

Copyright © 2022 Harita, Momi, Mazza and Griffiths. This is an open-access article distributed under the terms of the Creative Commons Attribution License (CC BY). The use, distribution or reproduction in other forums is permitted, provided the original author(s) and the copyright owner(s) are credited and that the original publication in this journal is cited, in accordance with accepted academic practice. No use, distribution or reproduction is permitted which does not comply with these terms.